HHS Public Access

Author manuscript

Mol Cancer Ther. Author manuscript; available in PMC 2024 October 02.

Published in final edited form as:

Mol Cancer Ther. 2024 April 02; 23(4): 492–506. doi:10.1158/1535-7163.MCT-23-0414.

Neutrophil elastase remodels mammary tumors to facilitate lung metastasis

Amriti R. Lulla[1], **Said Akli**[1], **Cansu Karakas**[1], **Joseph A. Caruso**[2], **Lucas D. Warma**[1], **Natalie W. Fowlkes**[3], **Xiayu Rao**[4], **Jing Wang**[4], **Kelly K. Hunt**[5], **Stephanie S. Watowich**[6,*], **Khandan Keyomarsi**[1,*]

[1]Department of Experimental Radiation Oncology, The University of Texas MD Anderson Cancer Center, Houston, TX, 77030, USA

[2]Department of Pathology and Helen Diller Cancer Center, University of California, San Francisco, CA 94143, USA

[3]Department of Veterinary Medicine and Surgery, The University of Texas MD Anderson Cancer Center, Houston, TX, 77030, USA

[4]Department of Bioinformatics and Computational Biology, The University of Texas MD Anderson Cancer Center, Houston, TX, 77030, USA

[5]Department of Breast Surgical Oncology, University of Texas MD Anderson Cancer Center, Houston, TX, 77030, USA

[6]Department of Immunology, University of Texas MD Anderson Cancer Center, Houston, TX, 77030, USA.

Abstract

Metastatic disease remains the leading cause of death due to cancer, yet the mechanism(s) of metastasis and its timely detection remain to be elucidated. Neutrophil elastase (NE), a serine protease secreted by neutrophils, is a crucial mediator of chronic inflammation and tumor progression. In this study, we used the PyMT model (NE+/+ and NE−/−) of breast cancer to interrogate the tumor-intrinsic and -extrinsic mechanisms by which NE can promote metastasis. Our results showed that genetic ablation of NE significantly reduced lung metastasis and improved metastasis-free survival. RNA-sequencing analysis of primary tumors indicated differential regulation of tumor-intrinsic actin cytoskeleton signaling pathways by NE. These NE-regulated pathways are critical for cell-to-cell contact and motility and consistent with the delay in metastasis in NE−/− mice. To evaluate whether pharmacological inhibition of NE inhibited pulmonary metastasis and phenotypically mimicked PyMT NE−/− mice, we utilized AZD9668, a clinically available and specific NE inhibitor. We found AZD9668 treated PyMT-NE+/+ mice showed significantly reduced lung metastases, improved recurrence-free, metastasis-free and overall survival, and their tumors showed similar molecular alterations as those observed in

[*]**Co-Corresponding authors:** Khandan Keyomarsi, The University of Texas, MD Anderson Cancer Center, 6565 MD Anderson Blvd, Unit 1052, Houston, TX 77030, Phone: +1-713-792-4845, kkeyomar@mdanderson.org, Stephanie S. Watowich, The University of Texas, MD Anderson Cancer Center, 1515 Holcombe Blvd, Unit 902, Houston, TX 77030, Phone: +1-713-792-4845, swatowich@mdanderson.org.

Conflicts of interest: All other authors declare no potential conflicts of interest.

PyMT-NE−/− tumors. Lastly, we identified a NE-specific signature that predicts recurrence and metastasis in breast cancer patients. Collectively, our studies suggest that genetic ablation and pharmacological inhibition of NE reduces metastasis and extends survival of mouse models of breast cancer, providing rationale to examine NE inhibitors as a treatment strategy for the clinical management of metastatic breast cancer patients.

Keywords

Neutrophil elastase; breast cancer; lung metastasis

Introduction

Despite decreases in triple-negative breast cancer (TNBC) death rates in recent years, little progress has been made in treating the disease once it metastasizes (1). The development of targeted therapies and select screening methods have significantly decreased the relapse rate and improved survival outcomes for patients with recurrent disease. Despite these advances, 20–30% of all TNBC patients die of metastatic disease, with no targeted therapies available (2). Hence, there is an unmet need for markers to predict recurrence and more effective targeted therapies.

Circulating neutrophils, as determined by the neutrophil-to-lymphocyte ratio (NLR), have been associated with worse survival in breast cancer patients (3). Neutrophils have been shown to establish pro-metastatic environments in murine models of breast cancer (4,5). Recent work has determined that neutrophils directly interact with breast cancer cells by secreting leukotrienes that selectively expand a highly tumorigenic subset of metastatic breast cancer cells in the lungs (6). These data suggest an important relationship between neutrophils and breast cancer metastasis, yet the mechanisms by which neutrophils promote metastatic disease remain largely unresolved.

Neutrophil elastase (NE), encoded by the *ELANE/Elane* gene (human/murine), is a serine protease that is expressed primarily by neutrophils. NE is stored in the azurophilic granules of neutrophils in homeostatic conditions. During inflammation and neutrophil activation, NE aids in the destruction of phagocytosed pathogens (7). In addition, NE can be released into the extracellular milieu and degrade extracellular matrix proteins (8). In this setting, NE carries out its chief physiological function of pathogen clearance, by enabling leukocyte migration and homing and recruitment of other immune cells to the inflammatory site (9–11). Hence, alteration in NE function can compromise the innate immune response, as seen in cases of severe congenital neutropenia, characterized by frameshift mutations in NE (12). However, dysregulated NE activity also contributes to a variety of pathological processes, including chronic obstructive pulmonary disease (COPD) (13), pulmonary fibrosis (14), atherosclerosis (15) and cancer (16). Hence, targeting NE for various pathologies is of interest in multiple disease processes.

In cancer, elevated NE levels have been correlated with disease progression in lung, colorectal, prostate and breast cancers (17–21). Previously, we have shown that NE can directly promote the growth of human breast tumor cells *in vitro* and murine mammary

tumors *in vivo* (22). Others have demonstrated that NE expression and activity in human breast tumors is associated with disease recurrence and metastasis (17). NE activity can be as high as three- to five-fold greater in cancer patients compared to those with COPD (23), driving inflammation and creating an ideal microenvironment for cancer progression in lung, colorectal, gastric and head and neck cancers (24–27). In all these studies, targeting NE significantly delayed tumor growth and blocked its pro-tumorigenic properties. Additionally, two studies have associated elevated NE levels with poor response to tamoxifen and trastuzumab in breast cancer patients (28). Despite being a consistent marker of poor outcomes, the NE-mediated mechanism(s) of tumor progression remain unresolved. Early studies with murine cancer models in lung, colon and Lewis lung carcinomas have suggested that NE could be critical in tumor initiation and growth (20,22,29–31). Being an integral component of neutrophil extracellular traps (NETs), NE is required for capturing circulating tumor cells and facilitating their seeding at the secondary metastatic site(s) (32,33). However, it remains unclear whether FDA-approved NE inhibitors, which are currently available for the treatment of COPD, could be effective in suppression of cancer metastasis. Based on these findings, we hypothesized that NE promotes breast cancer metastasis and could be genetically ablated or pharmacologically targeted to reduce metastatic disease.

In this study, we show NE-mediated effects in the breast tumor microenvironment have implications in metastasis. Using the PyMT breast cancer model of metastasis, we demonstrate that both the genetic and pharmacological blockade of NE decreases metastasis. Further, we show that blockade of NE is most effective following surgical removal of the primary tumor. Molecular analyses of NE-proficient and NE-deficient tumors identified a NE-modulated gene signature that can be used to predict metastasis in breast cancer patients. Collectively, our findings address a major gap in knowledge centered on elucidating the roles for NE in metastatic breast cancer and how pharmacological inhibition of NE can lead to inhibition of metastasis.

Materials and Methods

Patient samples and NE staining

For analysis of neutrophil elastase (NE) in breast tumors, 242 breast cancer patients with stage I-III breast cancer were enrolled in a prospective study between January 2000 and June 2010 (Lab00–222), approved by The University of Texas MD Anderson Cancer Center Institutional Review Board. Demographic, clinical, and pathologic data collected (see Supplementary Table S1) included age, stage at presentation, estrogen receptor (ER), progesterone receptor (PR), and human epidermal growth factor receptor 2 (HER2) status, tumor grade and disease status at last follow-up. Paraffin-embedded tissue blocks were obtained from each tumor and unstained slides were subjected to immunohistochemical (IHC) analysis with NE (monoclonal antibody NP57, DAKO, Agilent Technologies, Santa Clara, CA) as a marker for tumor associated neutrophils (TANs). IHC analysis was performed as described (22) with the exception that antigen retrieval was omitted for NE-IHC because it destroys the epitope recognized by the antibody. Tumor sections were blindly scored by two pathologists and positivity was defined as greater than 5 TANs per 40X high-power field; only NE-positive neutrophils within the tumor area were counted.

Animal models and survival surgery

FVB/N-Tg (MMTV-PyVT)634Mul/J (PyMT) (RRID:IMSR_JAX:002374) and (FVB/NJ RRID:IMSR_JAX:001800) mice were purchased from the Jackson Laboratory (Bar Harbor, ME).All animals used in this study have a fully functional immune system, without any perturbations to neutrophil function or tumor antigen burden and were housed in specific pathogen free (SPF) conditions, per provisions laid by AAALAC (Association for Assessment and Accreditation of Laboratory Animal Care) and IACUC (Institutional Animal Care and Use Committee) protocols (34,35).The generation of *Elane*$^{-/-}$ (herein referred to as NE−/−), have been previously described (36). The NE−/− mice, originally in C57BL/6 (RRID:MGI:2159769) (purchased from Jackson Laboratroies) were backcrossed to FVB/N strain of mice for 12 generations to generate the FVB/NJ, NE−/−, which along with FVB/NJ, wild-type (WT) were bred and maintained at the MD Anderson Cancer Center vivarium. To generate PyMT, NE−/− mice, FVB/NJ (NE−/−) mice were crossed with Tg (MMTV-PyVT) 634Mul (PyMT) mice. All animals were housed in a specific pathogen-free barrier facility with food and water ad libitum. For the spontaneous PyMT tumor models, animals were routinely monitored for tumor incidence starting at 6–8 weeks of age and tumor development was assessed by palpation. Routine tumor measurements were performed by calipers and the net tumor volume was calculated as (LXW^2) *0.5 mm^3. At endpoint, defined as the combined tumor volume (i.e. the sum of volumes of all mammary tumors in each mouse) reaching 1000mm^3, the total number of tumor-bearing mammary glands were evaluated, and tumors were harvested, weighed, and stored for IHC and molecular analyses. For orthotopic tumor models, female mice at 12–14 weeks were used for mammary tumor implantation. FVB NE+/+ and FVB NE−/− were implanted with viable tumor fragments (20–40 mm^3) harvested from PyMT NE+/+ and PyMT NE−/− mice, respectively. Tumor growth was measured using calipers and the net tumor volume was calculated as (LXW^2) *0.5 mm^3. For survival surgeries, tumors were allowed to grow to a size of 400–600mm^3 or for 10 days following the start of AZD9668 treatment (described below). Thereafter, primary tumors were resected surgically, and animals were allowed to recover for 14 days. Mice were then monitored for tumor recurrence and/ or decline of health. In case of tumor recurrence, mice were sacrificed if the tumor reached 1000mm^3 in size. At endpoint, lungs were harvested for metastasis evaluation as described below. Survival was assessed using Kaplan-Meier curves. Differences in survival between NE+/+ and NE−/− were measured using the log rank Mantel-Cox test. To establish experimental lung metastasis, $0.5X10^6$ 4T1 cells (RRID:CVCL_0125) were injected intravenously (i.v.) into the tail vein of 12 week old BALB/c mice. Animals were euthanized 14 days later, lungs were perfused with 10% formalin via tracheal instillation and harvested for analysis, as described below. All animal studies were approved by the Institutional Animal Care and Use Committee (IACUC) at the University of Texas MD Anderson Cancer Center.

Evaluation of lung metastasis

Lungs were harvested from all tumor-bearing mice, fixed overnight in 10% formalin, embedded in paraffin, sectioned, and stained with hematoxylin and eosin (H&E) as described previously (37). H&E-stained slides were scanned on the Aperio CS2 slide scanner (20X magnification) and subsequently analyzed for the number of metastatic foci in the lung sections using the counting tool on the Leica Imagescope v12.3 software. Lung

metastatic index (LMI) was calculated by determining the metastatic area/total lung area after manual annotation of metastatic tumor and unaffected lung using Leica Imagescope v12.3 software. Unpaired t-test with Welch's correction was used to assess differences as a function of NE status.

Fibroblast isolation, sorting and culture

Cancer-associated fibroblasts were isolated from tumors of PyMT NE+/+ and PyMT NE−/− mice, following the dissociation of tumor tissues as described (38) with the following modifications. Specifically, the single cell suspension (following homogenization as described above) was stained with 1:100 dilution of PE-conjugated CD140a(PDGFRα) antibody (RRID:AB_2715974) (catalogue number 135905; BioLegend), washed with FACS buffer and filtered through 40 μm cell strainers for sorting. CD140a+ve fibroblasts were sorted using the Aria II sorter (BD Biosciences) at the North Campus Flow Cytometry Core Laboratory of MDACC. Sorted fibroblasts were subsequently cultured on Corning® BioCoat® Collagen I-coated Plates (Catalog # 354400, Sigma) using RPMI 1640 media + 5% FBS. On reaching confluence, fibroblasts were harvested and used for RNA isolation and qRT-PCR.

TCGA and METABRIC breast cancer databases

In order to generate a NE-signature from the 12 genes identified in this study, The Cancer Genome Atlas (TCGA, https://www.cancer.gov/tcga) Breast Invasive Carcinoma PanCancer Atlas 2018 (https://www.cbioportal.org/study/summary?id=brca_tcga_pan_can_atlas_2018) and METABRIC (39), were interrogated, consisting of RNA-Seq and clinical data for 1082 and 1904 breast tissue samples, respectively (40). The data were processed with a modified version of CrossHub (41), a tool for the multi-way analysis of TCGA transcriptomic and genomic data. Log2 normalized gene expression as well as clinical data for both TCGA BRCA and METABRIC were downloaded from cBioPortal (https://www.cbioportal.org/) (42). For overall and recurrence-recurrence-free survival analyses, the median expression was used to define "high" and "low" expression cohorts for each gene and the NE-signature. Survival was assessed using Kaplan-Meier curves, and the log-rank test was used to define statistical differences.

AZD9668 treatments

AZD9668, whose structure and methods of synthesis were previously described (43), was synthesized by WuXi AppTec according to synthesis provided in its published patent from AstraZeneca, using the synthesis schema described in example 7 in the patent [(44) https://patentscope.wipo.int/search/en/detail.jsf?docId=WO2010094964). NMR spectrometry, LC-MS and HPLC analyses was performed to confirm the purity of and the metabolites profile of AZD9668 (Supplementary Data 1). All analyses show that the purity of the compound is 98–99.8%. For all experiments, AZD9668 was administered at a dose of 100mg/kg, B.I.D., by intraperitoneal (I.P.) injection (up to a 100μL injection per animal). The formulation of AZD9668 was: 20% DMSO, 60% PEG-400 and 20% water, per injection. Body weight and body mass were used to assess toxicity during the course of treatment. In case of signs of toxicity or distress, mice were given drug holidays till recovery. At the endpoint, toxicity

was assessed by evaluating the complete blood count panel from vehicle and AZD9668 treated animals.

Statistical analysis

All experiments were performed in triplicates and results were expressed as mean ± standard error (SE). Power analysis taking a 1:2 ratio between the NE−/− and NE+/+ animals, was used to determine the minimum number of mice to be used in each experiment. Data were analyzed using an unpaired t-test with Welch's correction with a p-value of <0.05 considered to be statistically significant. For all survival studies, Kaplan-Meier (KM) curves were used to determine differences between cohorts. The log-rank Mantel-Cox test was used to indicate statistically significant differences in KM curves.

The detailed procedures for elastin staining and quantification Isolation of immune cells (from tumors and peripheral tissues) and fibroblasts from tumors, flow cytometry and analysis, RNA sequencing, Reverse Phase Protein Array (RPPA) analysis, human cell xenograft studies, qRT-PCR, PK determination of AZD9668 Neutrophil Elastase activity are included in the Supplementary Materials and Methods.

Data Availability—The RNA-seq data generated from tumors from PyMT NE+/+ and PyMT NE−/− mouse models presented in this study have been deposited at the Gene Expression Omnibus repository: Accession numbers GSE217980.

Results

Neutrophil elastase (NE) positive TAN predict recurrence in breast cancer patients

To understand the role of NE in patients with invasive breast cancer, we examined the correlation between NE expression in breast tumor samples, patient outcomes and clinicopathologic parameters. For this study, we performed immunohistochemical (IHC) staining for NE on tumor samples from 242 patients diagnosed with stage I-III breast cancer, prospectively collected at The University of Texas MD Anderson Cancer Center (Figures 1A, 1B). Since NE expression is restricted to neutrophils and neutrophil precursors (45) NE positive tumors from patients were also called TAN high (i.e. positive) for all analysis. The median follow-up was 6.1 years; receptor status was as follows: 67% ER and/or PR positive; 15% HER-2 positive and 18% triple negative (Supplementary Table S1). For this patient cohort, full tumor blocks were available, allowing our pathologists to examine representative areas of tumor epithelium and include the peritumoral area where tumor-associated neutrophils (TANs), a major source of NE, often localize (Figure 1A). Positivity was defined as greater than 5 TANs per 40X high-power field (HPF) with only NE-positive neutrophils within the tumor area being counted. Breast tumors with high levels of TAN (TAN high and positive), defined as greater than 15 TANs per high-power field, were present in 45 of 242 tumors (19%) and correlated with a significantly poorer recurrence-free survival (RFS) compared with those tumors with low levels of TAN [i.e. TAN low (less than 15 per 40X HPF) or no TAN (TAN negative) (197/242 i.e. 81.4%)] (Figure 1B). High levels of TANs were significantly associated with low ER, low PR, TNBC status, high tumor grade, and disease recurrence on univariate analysis (Supplementary Table S1). Cox proportional

hazards analysis revealed that high levels of TAN were independently prognostic of RFS and were associated with a hazard ratio of 2.4 (95% CI, 1.1–5.5) for RFS (Supplementary Table S2).

Genetic ablation of NE inhibits breast cancer metastasis and extends survival in the PyMT model of breast cancer

To investigate NE involvement in breast cancer metastasis, we used a model that mimics the properties of human neutrophils, specifically elevated *Elane* enzyme activity as observed in human cancers (46,47). Mutations in the *Elane* gene, lead to misfolding of the protein and thus loss of enzyme activity. However, these mutations are primarily reported in cases of cyclic and severe congenital neutropenia (46). Such enzyme function altering mutations in *Elane* have not been reported in cancer thus far. On the contrary, there is increased *Elane* enzyme activity in tumors, none of which is attributed to *Elane* mutations (47). The autochthonous breast cancer murine model (PyMT), in which the polyoma virus middle T antigen is expressed specifically in mammary epithelial cells under the control of the mouse mammary tumor virus promoter closely mimics the human breast cancer model with comparable neutrophil elastase enzyme activity. Further, this model allowed for both genetic ablation and/or pharmacological inhibition of *Elane* and thus allows for testing the therapeutic benefits of no/low human NE enzyme activity in the tumor microenvironment, which was used in all our studies.

Female PyMT mice develop mammary gland hyperplasia by 6 weeks of age. The hyperplasia progresses through multiple stages of tumor development, mimicking human breast cancer (48,49). Mature female PyMT mice accumulate considerable metastatic burden in the lungs, which can be assessed by histology at 12 weeks of age. We bred PyMT mice (FVB background) with NE−/− mice, also in the FVB background, and subsequently monitored them and NE+/+ PyMT controls for breast cancer development and metastasis. Evaluation of pulmonary metastasis (the predominant distant site of metastasis (48)) in this PyMT model revealed that NE-deficiency significantly reduced the number of metastatic foci (range=1–8 foci in PyMT NE−/− mice, N= 14) compared to PyMT NE+/+ mice (range = 1–38 foci, N= 27) at 12 weeks of age (Figures 1C–1E). The size and number of metastatic foci in the lungs were diminished significantly in NE−/− mice (Fig. 1C–1E). Further, the incidence of metastasis was 90% (N=27/30 mice) in the PyMT NE+/+ background as compared to 66.6% (N=14/21 mice) in PyMT NE−/− mice (p=0.0389, Chi square analysis). Little (less than 2%) to no metastases were observed in other distant organs such as liver or bone marrow as previously described (50,51), as confirmed by evaluating the CD45-ve cells (putatively metastasized tumor cells) in bone marrows isolated from PyMT mice. CD45-ve cells accounted for less that 5% of all live cells, with no statistically significant differences between the two genotypes. (Supplementary Figure S1A).To confirm that the reduced metastasis was indeed a result of differential NE activity, we stained the lungs of both non-tumor-bearing and tumor-bearing mice with elastin, a cleaved substrate of NE (52) and thus correlative to NE activity and expression in tumors (53).

Under non-tumor bearing conditions, elastin levels in lung were comparable between FVB NE+/+ and FVB NE−/− mice (Supplementary Figure S1B). However, under tumor-bearing

conditions, elastin levels were significantly (p=0.02) higher in the lungs of PyMT NE−/− mice, suggesting that elastin was cleaved in lungs of PyMT NE+/+ mice (Figures 1F and 1G).

Lastly, to confirm that the effects of NE knockout are independent of the genetic background of the mice, we performed tail vein injections of 4T1 cells in BALB/c NE+/+ and BALB/c NE−/− mice. Fourteen days post-injection, we observed that BALB/c NE−/− mice had a 50% reduction in lung metastasis (p=0.006) compared to the BALB/c NE+/+ mice (Supplementary Figure S1C). Similar to the PyMT model, primary tumor growth was unaffected in the 4T1 model (BALB/c background) (Supplementary Figure S1D). No inherent differences in the neutrophil composition were observed between FVB NE−/− and BALB/c NE−/− mice (Supplementary Figure S1E). These data suggest NE promotes breast cancer metastases in the lungs, regardless of genetic background of the mice.

To assess the effect of NE on primary breast tumors, we evaluated whether NE altered normal or malignant growth in the mammary glands. We did not detect differences in mammary gland development in non-tumor bearing NE+/+ and NE−/− FVB mice, as assessed by mammary fat pad filling by the epithelial tree (Supplementary Figure S1F), suggesting minimal if any role for NE in normal mammary gland development. Additionally, NE did not affect primary tumorigenesis as assessed by the percentage of tumor-free mice over time (Supplementary Figure S2A). Mammary tumors were also collected from the PyMT NE+/+ and PyMT NE−/− mice at endpoint of 14–16 weeks and tumors were measured revealing that both genotypes had comparable tumor burden (Supplementary Figure S2B). Further, the number of mammary gland bearing tumors per mouse, was not statistically different between the two genotypes and the tumors had similar doubling times (Supplementary Figure S2C and S2D), respectively. Collectively, these data provide evidence that NE has minimal effect on primary breast tumor development and growth. We also examined the histology of the primary tumors in PyMT NE+/+ and PyMT NE−/− models. Assessment of hematoxylin and eosin (H&E) stained sections of these tumors revealed four major histologies- solid, alveolar/tubular, papillary and adenosquamous (54), at similar frequencies between both genotypes (Supplementary Figure S2E). Collectively, these data indicate that while NE promotes lung metastasis, it has minimal effect on primary breast tumor development and growth.

NE-mediated inhibition of lung metastasis extends recurrence-free survival in the orthotopic PyMT model of breast cancer

To assess the impact of NE on lung metastasis, independent of the primary tumor growth, we examined if the ablation of NE in a post-surgical setting affected metastasis-free survival. To this end, we orthotopically implanted PyMT tumors in the mammary fat pads of FVB NE+/+ and FVB NE−/− mice and subsequently performed survival surgery to allow metastatic growth in the absence of the primary tumor. Once the tumors reached 400–600 mm^3 in size (40–50% of the size of the spontaneous tumors at 12 weeks), the primary tumor was resected (survival surgery) and mice were followed for tumor recurrence, metastasis, and health decline (Figure 2A). Primary tumors were comparable is size between the NE+/+ and NE−/− genotypes at resection (Supplementary Figure S2F). The findings demonstrate that

tumors in both genotypes required approximately 50 days to attain an average volume within the range of 400–600mm^3, a critical threshold for conducting survival surgeries. Tumor recurrence occurred in 70% of the NE+/+ group post resesection. Strikingly, post survival surgery, removal of NE significantly prolonged (by 5-fold) survival of FVB NE−/− mice compared to FVB NE+/+ mice (overall survival= 270 days vs 46 days, respectively, Figure 2B). Moreover, the time to lethal metastatic burden development was significantly shorter in FVB NE+/+ mice. Specifically, metastasis related events were significantly delayed in FVB NE−/− mice (metastasis-free survival = 345 days) compared to FVB NE+/+ mice, whereby day 46, 11 out of the 12 mice succumbed to death due to metastasis (Figure 2C). Further, evaluating the extent of metastasis, as measured by lung metastatic index (LMI), showed that 84% of FVB NE+/+ mice died of LMI >5% (at 46 days), compared to 54% in the FVB NE−/− at the one-year mark (Figure 2D). H&E analysis of lung tissue (day 46) showed that metastatic tumors in FVB NE+/+ mice were carcinomas that colonized the entire lung (i.e. entire normal lung parenchyma). By contrast, metastatic tumors in FVB NE−/− mice (day 176) tended to be adenomas that did not colonize all lobes of the lungs (Figure 2E). Collectively, these results suggest that ablation of NE activity benefits survival outcomes and reduces the severity of metastatic disease following primary tumor resection.

Immune responses in PyMT tumors are NE independent

To understand whether NE altered immune composition in tumors, lungs, or hematopoietic organs, we performed immune profiling studies in 12–14 weeks PyMT NE+/+ (n=5) and PyMT NE−/− (n=5) mice. Only neutrophil accumulation in mammary tumors was modestly mediated in part by NE, as judged by the reduced number of neutrophils found in tumor tissue volumes (i.e., counts per mg tissue) in PyMT NE−/− versus PyMT NE+/+ animals (Supplementary Figure S3A, Supplementary Tables S3 and S4). All other immune subsets were comparable between PyMT NE+/+ versus PyMT NE−/− mice; neutrophil frequencies within the CD45+ population and the proportion and absolute number of other immune populations analyzed were not affected by NE (Supplementary Figure S3B). Since the numbers of immune cells between the two genotypes were unchanged, we examined if there are any T cell specific changes between the immune subsets in each genotype. T-cells were assessed using a focused T-cell antibody panel consisting of markers such as PD-1, Tregs, naïve and memory cells in each of the CD4 and CD8 T-cell population. We hypothesized that if T-cells were indeed playing a role in inducing metastasis as a function of NE, then in the NE−/− mice, a greater CD8 T-cell accumulation could be associated with reduced metastasis. However, the analysis revealed that there were no statistically significant differences between the naïve and effector CD4 or that of CD8 T-cells, nor was there a significant change in the PD-1 expression or any changes in Tregs between the two genotypes (Supplementary Figure S4). Thus, T-cells were comparable between the PyMT NE+/+ and PyMT NE−/− mice. Furthermore, no significant NE specific changes [by percent or absolute counts] in monocytes or tumor associated macrophage populations were detected between the two genotypes (Supplementary Figure S3). Taken together, this data suggests that the differential metastasis between PyMT NE+/+ and PyMT NE−/− is unlikely to be attributed to tumor inflammatory pathways.

NE mediates transcriptional alterations in cytoskeletal signaling pathways in PyMT tumors

Given the similarities in the immune milieu of both genotypes, we next examined if there were proteomic differences as a function of NE in the clinical setting. The correlation between the NE-positive infiltrate and cancer cell signaling pathways was examined by subjecting tumor lysates from the 242 patients (from Figure 1) who had fresh frozen tissue available for RPPA (Reverse Phase Protein Array) analysis (Supplementary Figure S5A). Comparison of breast tumors with high expression for TAN (45/242) and breast tumors with low expression for TAN (197/242) using the Mann-Whitney *U*-test revealed differences in the abundance of several signaling intermediates (Supplementary Figure S5B). High levels of p90RSK phosphorylated at threonine 359/serine 363 (phosphorylation catalyzed by ERK) and Rb phosphorylated at serine 807 were strongly associated with the presence of NE-high TAN (Supplementary Figure S5A). However, while both p90RSK -pT359/S363 and Rb proteins have key roles in cell cycle signaling pathways, neither protein is a direct substrate of NE that could enhance metastasis. These results suggest that NE likely may have two roles, one through the activation of cell cycle/signaling pathways and the other by reprogramming the transcriptional roles of NE in the metastatic setting. To interrogate this hypothesis, we examined RNA expression profiles of mammary tumors resected from PyMT NE+/+ (n=5) and PyMT NE−/− (n=5) mice (12 weeks of age). Flow cytometry analysis of the dissociated tumor tissue showed that epithelial cells comprised more than 95% of the isolated PyMT tumors in both genotypes (Supplementary S6A) and hence the RNA-seq results are primarily representative of mammary tumor (i.e. epithelial) cells. Using a cutoff of p-value <0.05 (adjusted p-value 0.34) and absolute fold change of >2.0, RNA-seq analysis identified 560 significant differentially expressed genes (DEGs), between the two cohorts, as depicted by heatmap of these DEGs per mouse (Fig 3A) and by volcano plot per cohort (Fig 3B). The 560 DEGs (166 upregulated and 394 downregulated) were subjected to Ingenuity Pathway Analysis (IPA). This revealed multiple pathways that affect cytoskeletal signaling in cancer cells, including Actin cytoskeleton signaling, Rho kinase signaling, Paxillin signaling and ILK signaling, which were among the top enriched pathways in PyMT NE−/− tumors (Figure 3C). Collectively, these pathways contribute to the cell matrisome (55). Gene ontology (GO analysis) using the PANTHER database (56) confirmed that 123 of the 560 DEGs belonged to the matrisome class of proteins (22% of DEGs) (Figure 3D), with ECM and cytoskeletal proteins contributing to the majority of the DEGs identified within the 123 gene subset. Examination of these 123 genes in the Matrisome database (57) (http://matrisomeproject.mit.edu/) further subclassified these genes into secreted factors and ECM proteoglycans (Figure 3E), which are critical for cell-to-cell communication and motility.

We next validated the 32 key genes within each of the pathways represented in the 123 gene subset (all in the Matrisome protein class) by qRT-PCR analysis. These experiments identified 19 genes (Supplementary Table S5) that were significantly altered in PyMT NE+/+ (n=5) as compared to PyMT NE−/− (n=6) tumors (Figure 4A). Of these 19 genes, 9 genes were significantly upregulated and 3 were significantly downregulated (including SERPIN11B, PRTN2 and LEF1) in NE-deficient mice in both the preneoplastic mammary glands (Supplementary Figure S6B) and PyMT tumors (Figure 4A), suggesting their NE-specific role in the tumor microenvironment. Due to the contribution of cancer-associated

fibroblasts (CAFs) in the alteration of cellular cytoskeletal proteins, specifically in the dissemination and migration of cancer cells (58), we next set out to evaluate if the CAFs were a predominant component of the RNA-seq data generated from the tumor tissues. To this end, we quantitated the CAF specific CD140+ cells in PyMT NE+/+ and PyMT NE−/− tumors by flow cytometry and found that CAFs contributed to only 1% or less of the total tumor population (Supplementary Figure S6C). Thus, the RNA-seq signature generated from our studies was primarily attributed to tumor cells. Lastly, despite that CAFs were only 1% of the total tumor population, we validated their gene signature by isolating CAFs from PyMT NE+/+ (n=4) and PyMT NE−/− (n=4) tumors (Figure 4B). These analyses revealed significant overexpression of *IL33* (5-fold) in CAFs from PyMT NE−/− tumors compared to PyMT NE+/+ tumors. IL33 is a known substrate of NE (59), and its cleaved forms have recently been shown to be upregulated in metastases-associated fibroblasts in mouse models of spontaneous breast cancer metastasis and in patients with breast cancer with lung metastasis. qRT-PCR enables the measurement of unprocessed (uncleaved) RNA transcripts of IL33 at the molecular level. Consequently, the levels of these unprocessed RNA transcripts are expected to increase in NE−/− models, as depicted in Figure 4B.

A NE−/− specific signature predicts for favorable recurrence-free and overall survival in breast cancer patients

Based on our findings that NE-deficient mice have significantly longer metastasis-free survival (Figure 2), we next hypothesized that the NE specific gene signature, which we derived from our mouse models, can be used to predict recurrence-free survival (RFS), progression-free survival (PFS) and overall survival (OS) in breast cancer patients. To this end, we interrogated the METABRIC (39,40) and the Cancer Genome Atlas (TCGA) (60) databases for RNA expression of the 12 genes that we had identified as downregulated by NE (Figure 4A) in primary breast tumors. Specifically, we hypothesized that patients presenting with higher expression of the 12 NE-downregulated genes are likely to have better outcomes, compared to those with lower expression. Using median RNA expression as the cut-off, patients were thereafter stratified as “low” and “high” for each gene. We only included those patients with either all high or all low expression in each of the 12 genes and evaluated RFS and OS (METABRIC), or PFS and OS (TCGA) for the breast cancer patient cohorts in each database. An NE-specific gene signature was then generated using the genes that showed significant differences in RFS/OS or PFS/OS for individual genes, in each database (Supplementary Figure S7). As seen in Figures 4C–4F, 4 of the 12 NE-downregulated genes predicted outcomes. Specifically, IL33, MYBPC1 and TNNT3 were predictors of OS and RFS in the METABRIC dataset, while IL33, MYBPC1 and TRIM63 were predictors of OS and PFS in the TCGA dataset (Figure 4E, 4F). The outcome data for RFS in METABRIC or PFS in TCGA databases revealed that “high” expression cohorts experienced a significant survival benefit of 5 and 4 years in METABRIC (p=0.0016) and TCGA (p=0.0002), respectively. Similarly, the outcome data for OS in both databases revealed that “high” expression cohorts experienced a significant survival benefit of 8.2 and 1.3 years in METABRIC (p<0.0001) and TCGA (p=0.0019), respectively. The combined 3-gene signature was a better predictor of both RFS and OS, compared to any gene alone in each of the databases (Supplementary Figures S7A–S7D). Collectively, the patient data reveal that elevated expression of IL33, MYBPC1 and TNNT3 in METABRIC, and IL33,

MYBPC1 and TRIM63 in TCGA, can be used to predict the likelihood of RFS or PFS and OS in breast cancer patients, suggesting NE-regulated pathways affect breast cancer survival outcomes.

Pharmacologic inactivation of NE inhibits lung metastasis

The striking inhibition of metastasis upon genetic removal of NE in PyMT mice (Fig. 1C and D), suggested an opportunity for translation of these findings using an NE inhibitor, AZD9668 (61). AZD9668 is an orally active and fully reversible inhibitor of NE (43) that has been used in phase I and II clinical trials in patients with chronic obstructive pulmonary disease (COPD) (62–64). AZD9668 is well tolerated at single doses up to 150mg and multiple doses up to 70mg twice daily in both healthy volunteers as well as those patients with COPD, and adverse events were similar for AZD9668 and placebo in these clinical trials (62–64). To date, AZD9668 has not been used for the treatment of patients diagnosed with cancer. Due to the key roles of NE in breast cancer growth and metastasis we hypothesized that AZD9668 would be an effective therapy for inhibiting breast cancer metastasis in the autochthonous PyMT-NE+/+ model. We found effective dosing and NE inhibition in mice using AZD9668 administration [Intraperitoneal (IP)] at 100mg/kg daily (Supplementary Figure S8A). Moreover, AZD9668, but not AZD5069, a reversible inhibitor of CXCR2 (the chemokine receptor for NE, also used for the treatment of COPD) (65) inhibited NE in cell-free NE activity enzyme assays (Supplementary Figure S8B).

To test whether AZD9668 suppressed pulmonary metastasis, we treated PyMT-NE+/+ mice with AZD9668 (100mg/kg, BID, IP) or DMSO (n=11 in each treatment arm). Treatment was initiated at 7 weeks of age and was maintained for up to 14 weeks age. Mice were sacrificed as tumors reached the maximum allowable tumor burden or a moribund state, at which point mammary tumors and lungs were harvested for analysis. Percent tumor-free mice in PyMT NE+/+ mice was unaffected by AZD9668 treatment, with comparable tumor incidence as function of time noted as in the vehicle-treated mice (Figure 5A). Doubling times of PyMT tumors and endpoint tumor burden were also comparable between the vehicle and AZD9668 treated cohorts (Figures 5B–5C). AZD9668 treatment was also well tolerated, resulting in no significant changes in body weight vs. controls (Supplementary Figure S8C). We also examined the cellular substrates of AZD9668 by measuring the expression of TSP-1 (a specific substrate of NE (4,32)) in both PyMT NE+/+ versus PyMT NE−/− mice as well as AZD9668 versus vehicle treated FVB NE+/+ mice. As seen in the western blot analysis presented in Supplementary Figure S8D, we show that TSP-1 expression is low to undetectable in the tumors derived from PyMT NE+/+ mice, but the levels increase in each of the tumors derived from PyMT NE−/− mice, showing that in the absence of NE, TSP-1 is protected from being degraded. Similarly, when we treated the FVB mice transplanted with the PyMT NE+/+ tumors with AZD-9668, TSP-1 protein was protected from degradation seen in the vehicle treated tumors (Supplementary Figure S8E).

Strikingly, histological assessment of the lungs revealed reduced metastatic burden in mice treated with AZD9668 compared to DMSO-treated controls (Figure 5D). Moreover, the number of lung metastatic foci (Figure 5E) were significantly fewer and the percentage of tumor area to normal lung parenchyma (Figure 5F) in AZD9668-treated mice were

appreciably smaller compared with vehicle-treated mice (0.49+/−0.21% vs. 0.03+/−0.01%, p=0.05). These results indicate that the pharmacological inhibition of NE using AZD9668 treatment significantly inhibits breast cancer pulmonary metastasis in PyMT mouse model with similar efficacy as genetic deletion of NE.

Studies in the immune competent PyMT model were confirmed using immune compromised xenograft models of human cell lines MDA-MB-231 and MDA-MB-468. In these xenograft models, treatment with AZD9668 significantly delayed primary tumor growth (Supplementary Figure S9A–B) concomitant with reduced BrDU incorporation, suggesting fewer cells in the S-phase of the cell cycle (Supplementary Figures S9C and S9D). Quantitation of BrDU staining indicated these differences were statistically significant between vehicle and AZD9668 treatment arms (Supplementary Figures S9E–F).

To assess if AZD9668 impacts cytoskeletal signaling in the tumor microenvironment, we interrogated expression of the 19 gene signature we identified (Figure 4A). Of these, 13 genes were significantly altered in AZD9668 treated tumors, including NE-specific genes, similar to changes observed the NE-deficient mice (Figure 5G). Moreover, the same four NE-downregulated genes (IL33, Mybpc1, Tnnt3 and Trim63) shown to predict favorable RFS or PFS and OS in breast cancer patients (Figure 4 C–F) were also expressed at greater amounts in the PyMT tumors from AZD9668-treated mice (Figure 5G), in agreement with their inhibition by NE. Thus, overall, the NE-specific inhibitor AZD9668 replicates the phenotypic and molecular changes observed in PyMT-NE−/− mice.

We next examined the impact of AZD9668 treatment on lung metastasis, independent of primary tumor growth. To this end, we assessed if pharmacological inhibition of NE in a post-surgical setting affected metastasis-free survival (Figure 6). PyMT NE+/+ tumors were orthotopically transplanted into 30 FVB NE+/+ mice and, following 7–10-day recovery time from surgery, mice were treated with AZD9668 (100 mg/kg BID, IP) or DMSO for 10 days, at which point the primary tumors reached 400–600 mm^3. The primary tumors were resected, and mice were treated for an additional 90 days with either AZD9668 (100mg/kg, BID, IP) or DMSO. At the end of 90 days, treatments were discontinued, and mice were monitored for recurrence and/or death due to metastasis (see the experimental flow, Figure 6A). Survival studies showed that AZD9668 treatment of NE+/+ tumors effectively mimicked genetic NE-deficiency. Specifically, results revealed that treatment of mice with AZD9668 increased time to median OS from 94 days (vehicle/DMSO) to 464 days (Figure 6B). Similarly, for metastasis-free survival, the endpoint was not achieved in the AZD9668 treated mice, while majority of the vehicle/DMSO mice succumbed to metastasis by day 91 (Figure 6C). One observation that was distinct between the AZD9668 treated and NE-deficient mice was that, upon treatment with AZD9668, mice were either non-responders (succumbed to metastasis within the first 100 days post survival surgery) or were super-responders (only 1–3 events (i.e. deaths) between days 100–400 post survival surgery). In the NE-deficient mice, there were no such groups observed, with the majority of the mice starting to decline later than 120 days from survival surgery.

We also evaluated RFS (for primary tumor alone) and observed that AZD9668 treated mice had fewer primary tumor recurrences compared to vehicle treated mice (RFS=

53 days for vehicle/DMSO vs. not achieved for AZD9668) (Figure 6D). Lastly, at the molecular level, even 10 days of treatment with AZD9668 resulted in alteration of expression of cytoskeletal genes with the levels of all the 19 genes (from Figure 4) including the four NE-downregulated biomarker genes (IL33, Mybpc1, Tnnt3 and Trim63) increasing following treatment (Figure 6E). Collectively, our studies suggest that treatment with AZD9668 mimics NE-deficiency and induces similar transcriptional alterations in cytoskeletal signaling within the breast tumor microenvironment.

Discussion

The most common cause of death in breast cancer patients is due to metastasis. Furthermore, it is not clear whether the current systemic therapies are eradicating micro-metastasis (metastatic disease) or just eliminating local-regional disease and therefore preventing metastasis. In this study, we demonstrate that NE promotes pulmonary metastasis in the PyMT autochthonous mouse model of breast cancer. This presents a rationale for therapeutically inhibiting NE with AZD9668, an NE inhibitor already used in multiple clinical trials for various lung diseases (61). Strikingly, AZD9668 significantly repressed PyMT lung metastases, suggesting the potential to directly target human pulmonary breast cancer metastasis with this agent. Furthermore, based on NE effects on tumor gene expression, we generated a NE-related gene signature encompassing 4 genes downregulated by NE (IL33, Mybpc1, Trim63 and Tnnt3), which predict outcomes in breast cancer patients and may be useful in monitoring response to AZD9668.

Several previous studies have demonstrated that NE significantly impacts tumor progression by inhibiting tumor growth and/or preventing tumor development in various mouse models of cancer (20,22,29–31). Mechanistically, these growth inhibitory functions of NE can be attributed to either NE-mediated activation of mitogenic pathways such as the EGFR-MAPK signaling (22) or NE-mediated inhibition of tumor suppressors such as IRS-1, EMILIN1.

In contrast to the pro-tumorigenic roles of NE we describe in our current study, a recent report from Cui et al (66) described the apoptotic role of NE, as a mechanism of preventing tumorigenesis. While the authors elegantly demonstrate apoptosis using PMN cultures, there are several differences between our two studies that have led to different outcomes and conclusions: 1) All the PMN cultures in the Cui study were derived from “healthy volunteers” and not cancer patients. Thus, the apoptosis phenomenon is not surprising, given the inherent nature of neutrophils to recognize and kill any foreign entity (67). PMNs from healthy volunteers, in most circumstances, are naïve to cancer cells and have not been re-programmed like the neutrophils in the tumor microenvironment. Thus, the primary foreign entity or antigen was missing in these studies. 2) Most of the *in vitro* and *in vivo* studies performed used their PMN cultures in short-term experiments. Reprogramming of immune cells in the tumor microenvironment is a gradual process in tumorigenesis (68) and hence, the Cui study may only be representative of early anti-tumorigenic properties of NE, perhaps even before primary tumors are completely developed. 3) The dose of NE used and the mode of delivery in tumors (intratumoral injection) are not physiological or clinically achievable. It is likely that at physiological doses of NE, it has pro-tumorigenic effect, however at the higher doses, that surpasses physiological levels, that NE shifts to

becoming cytotoxic. Hence, the apoptosis responses observed in the Cui paper may not be a direct consequence of neutrophils releasing NE when exposed to cancer cells, examines short term effects and early stages in tumorigenesis, and not translatable to experimental systems at physiological doses of NE that can impact metastasis.

In our study, we observed no differences in tumor incidence or tumor growth between the PyMT NE+/+ and PyMT NE−/− transgenic mice (Supplementary Figure S2A, B), and only a slight, albeit not statistically significant, increase in growth rate in the transplanted PyMT NE−/− tumors compared to PyMT NE+/+ tumors (Supplementary Figure S2F). However, NE was consistently critical for lung metastasis and tumor recurrence in our mouse models (Figures 1 and 2), demonstrating its role beyond primary tumor growth. Molecular analysis of tumors derived from PyMT-NE−/− and PyMT-NE+/+ mice further validated our findings, where no significant alterations were found in cell cycle and other tumor proliferation pathways (Figure 3). Moreover, the immune milieu between PyMT-NE−/− and PyMT-NE+/+ tumors was similar (Supplementary Figure S3 and Supplementary Figure S10), thus indicating that there are underlying properties intrinsic to the tumor microenvironment (TME) that promote metastasis in an NE-sufficient background. Of note, neutrophil frequencies within the CD45+ population were not affected by NE (Supplementary Figure S3B), suggesting that changes in NE mediated transcriptional reprogramming of the primary tumors is not likely mediated by changes in neutrophils. Transcriptomic and IPA analysis revealed that cytoskeleton pathways were the main differentially regulated pathways between the PyMT-NE−/− and PyMT-NE+/+ tumors (123 DEG's, 65% up-regulated and 35% downregulated, Figure 3B). While these genes and pathways identified in our study are "protumorigenic" and "prometastatic", that these pathways are also critical in TME for contractility and expansion of tissues. In the context of NE−/−, the hypothesis emerging from these analysis is that the absence of NE increases signaling in these pathways to promote more contractility, by activating the contractile proteins. This limits motility and hence an "up-regulation" of these genes are observed. In fact, qRT-PCR analysis of CAFs further indicated that NE-specific substrates such as IL33 could be differentially secreted in the TME, thus aiding the differential cytoskeletal composition of the PyMT tumors in the NE−/− vs. NE+/+ backgrounds. (Figure 3).

The cellular cytoskeleton, composed primarily of actin and myosins, is known to aid tumor progression and metastasis by regulating cell polarity, adhesion, and migration (69,70). NE is also one of the most diverse proteolytic enzymes whose roles in both NET (71) and TME remodeling have been described in multiple studies (32,72,73), but these roles of NE are not restricted to just one mechanism. For example, NE can promote angiogenesis by cleaving VEGF and PDGF in esophageal cancers (72). Similarly, NE specific proteolysis of proteins such as P-selectin (73), laminin and TSP-1 (32) have been noted in previous reports and shown in our study (Supplementary Figures S8D and S8E), each leading to a distinct phenotype (e.g. transmigration, tumor growth, tumor cell adhesion etc.) in the corresponding mouse models. TSP-1's function goes beyond being a NE specific substrate as it has been implicated in migration and invasion as a function of cyclin D1 expression (74). Hence, there is not just one mechanism by which NE can remodel the TME. Our study provides the novelty in that we show that the TME remodeling is not restricted to the proteolytic or NET functions of NE, but is also seen at the transcriptomic level. The survival surgery

data (Figure 2) demonstrates that long-term absence of NE not only delays metastasis, but also reduces the grade of recurred tumors. Thus, the transcriptomic reprogramming of tumors is a key mechanism that we propose based on the data presented in our study. Our data also suggests that NE-deficient tumors have increased cytoskeletal activity compared to NE-proficient tumors, which may prevent the NE-mediated “loosening” of the TME that enables cancer cells to more readily leave the TME and metastasize. Specifically, the genes IL33, Mybpc1, Tnnt3 and Trim63 form an NE-downregulated gene signature that can distinguish tumors that are more likely to metastasize. Retrospective analyses of primary tumors using the TCGA and METABRIC datasets revealed that the four-NE-downregulated gene signature can be used as potential biomarkers to predict recurrence-free or progression-free survival as well as overall survival (Figure 4).

In addition to identifying an NE-regulated gene signature that can predict breast cancer patient outcomes, we also show that pharmacological inhibition of NE (by AZD9668) significantly reduces pulmonary metastasis and primary tumor recurrence and improves overall and metastasis-free survival in PyMT-NE-sufficient tumors. Our study demonstrates the effective use of NE inhibitors in the adjuvant setting i.e. post primary tumor resection. We are proposing the use NE inhibitors alongside of standard of care in patients in future clinical trials. AZD9668 has been well tolerated in our animal model. Moreover, AZD9668 has been shown to be well tolerated in healthy individuals and was found to possess favorable pharmacokinetics in phase I clinical trials (62). In phase II clinical trials, AZD9668 did not alleviate the symptoms of COPD patients (64) and had limited benefit in patients with bronchiectasis and cystic fibrosis (75). However, AZD9668 diminished levels of pro-inflammatory biomarkers in the bloodstream and levels of NE-specific elastin catabolites, desmosine and isodesmosine in the urine of patients (75) and inhibited patient-derived neutrophils (76). Oral administration of AZD9668 to rats or mice prevented NE-induced lung injury and reduced inflammation following exposure to cigarette smoke (76). These findings, together with those we present in this report, suggest that AZD9668 may be an effective inhibitor of NE in breast cancer.

In summary, we provide evidence that NE is an important factor contributing to the pro-metastatic role of neutrophils in breast cancer. Using AZD9668, we show that pharmacological inhibition of NE greatly reduces pulmonary metastasis and improves overall and metastasis-free survival in the PyMT mouse models of breast cancer. Since AZD9668 has already been shown to be safe and tolerable in patients, this finding is highly actionable and has the potential to address the unmet clinical need of treating metastasis in breast cancer.

Supplementary Material

Refer to Web version on PubMed Central for supplementary material.

Acknowledgements

We thank Dr. Philip Jones from Institute for Applied Cancer Science for facilitating the synthesis and pharmacokinetics studies of AZD9668. Research reported in this manuscript was supported by Cancer Prevention Research Institute of Texas (CPRIT) #RP180181 to SSW and KK, by CPRIT - Multi-Investigator Research Award

#RP180712 to KKH and KK, by the National Cancer Institute (NCI) R01CA223772 and R01CA255960 to KK, by CPRIT Research Training Program grant RP170067 and RP210028 to LDW and by the NCI through MD Anderson's Cancer Center Support Grant (P30CA016672).

K.K. Hunt is on the medical advisory board for Armada Health and AstraZeneca and receives research funding to MD Anderson Cancer Center from Cairn Surgical, Eli Lilly & Co, and Lumicell.

References

1. Siegel RL, Miller KD, Jemal A. Cancer statistics, 2020. CA Cancer J Clin 2020;70(1):7–30 doi 10.3322/caac.21590. [PubMed: 31912902]
2. Early Breast Cancer Trialists' Collaborative G. Effects of chemotherapy and hormonal therapy for early breast cancer on recurrence and 15-year survival: an overview of the randomised trials. Lancet 2005;365(9472):1687–717 doi 10.1016/S0140-6736(05)66544-0. [PubMed: 15894097]
3. Ethier J-L, Desautels D, Templeton A, Shah PS, Amir E. Prognostic role of neutrophil-to-lymphocyte ratio in breast cancer: a systematic review and meta-analysis. Breast Cancer Research 2017;19(1):2 doi 10.1186/s13058-016-0794-1. [PubMed: 28057046]
4. El Rayes T, Catena R, Lee S, Stawowczyk M, Joshi N, Fischbach C, et al. Lung inflammation promotes metastasis through neutrophil protease-mediated degradation of Tsp-1. Proc Natl Acad Sci U S A 2015;112(52):16000–5 doi 10.1073/pnas.1507294112. [PubMed: 26668367]
5. Coffelt SB, Kersten K, Doornebal CW, Weiden J, Vrijland K, Hau CS, et al. IL-17-producing gammadelta T cells and neutrophils conspire to promote breast cancer metastasis. Nature 2015;522(7556):345–8 doi 10.1038/nature14282. [PubMed: 25822788]
6. Wculek SK, Malanchi I. Neutrophils support lung colonization of metastasis-initiating breast cancer cells. Nature 2015;528(7582):413. [PubMed: 26649828]
7. Belaaouaj A, McCarthy R, Baumann M, Gao Z, Ley TJ, Abraham SN, et al. Mice lacking neutrophil elastase reveal impaired host defense against gram negative bacterial sepsis. Nature medicine 1998;4(5):615.
8. Colom B, Bodkin JV, Beyrau M, Woodfin A, Ody C, Rourke C, et al. Leukotriene B4-Neutrophil Elastase Axis Drives Neutrophil Reverse Transendothelial Cell Migration In Vivo. Immunity 2015;42(6):1075–86 doi 10.1016/j.immuni.2015.05.010. [PubMed: 26047922]
9. Henry CM, Sullivan GP, Clancy DM, Afonina IS, Kulms D, Martin SJ. Neutrophil-Derived Proteases Escalate Inflammation through Activation of IL-36 Family Cytokines. Cell Rep 2016;14(4):708–22 doi 10.1016/j.celrep.2015.12.072. [PubMed: 26776523]
10. Kessenbrock K, Frohlich L, Sixt M, Lammermann T, Pfister H, Bateman A, et al. Proteinase 3 and neutrophil elastase enhance inflammation in mice by inactivating antiinflammatory progranulin. J Clin Invest 2008;118(7):2438–47 doi 10.1172/JCI34694. [PubMed: 18568075]
11. Young RE, Thompson RD, Larbi KY, La M, Roberts CE, Shapiro SD, et al. Neutrophil elastase (NE)-deficient mice demonstrate a nonredundant role for NE in neutrophil migration, generation of proinflammatory mediators, and phagocytosis in response to zymosan particles in vivo. J Immunol 2004;172(7):4493–502 doi 10.4049/jimmunol.172.7.4493. [PubMed: 15034066]
12. Horwitz MS, Corey SJ, Grimes HL, Tidwell T. ELANE mutations in cyclic and severe congenital neutropenia: genetics and pathophysiology. Hematol Oncol Clin North Am 2013;27(1):19–41, vii doi 10.1016/j.hoc.2012.10.004. [PubMed: 23351986]
13. Shapiro SD, Goldstein NM, Houghton AM, Kobayashi DK, Kelley D, Belaaouaj A. Neutrophil elastase contributes to cigarette smoke-induced emphysema in mice. Am J Pathol 2003;163(6):2329–35 doi S0002–9440(10)63589–4 [pii] 10.1016/S0002-9440(10)63589-4. [PubMed: 14633606]
14. Gregory AD, Kliment CR, Metz HE, Kim KH, Kargl J, Agostini BA, et al. Neutrophil elastase promotes myofibroblast differentiation in lung fibrosis. J Leukoc Biol 2015;98(2):143–52 doi 10.1189/jlb.3HI1014-493R. [PubMed: 25743626]
15. Alfaidi M, Wilson H, Daigneault M, Burnett A, Ridger V, Chamberlain J, et al. Neutrophil elastase promotes interleukin-1beta secretion from human coronary endothelium. J Biol Chem 2015;290(40):24067–78 doi 10.1074/jbc.M115.659029. [PubMed: 26269588]

16. Sato T, Takahashi S, Mizumoto T, Harao M, Akizuki M, Takasugi M, et al. Neutrophil elastase and cancer. Surg Oncol 2006;15(4):217–22. [PubMed: 17320378]
17. Akizuki M, Fukutomi T, Takasugi M, Takahashi S, Sato T, Harao M, et al. Prognostic significance of immunoreactive neutrophil elastase in human breast cancer: long-term follow-up results in 313 patients. Neoplasia 2007;9(3):260–4. [PubMed: 17401466]
18. Lerman I, Garcia-Hernandez ML, Rangel-Moreno J, Chiriboga L, Pan C, Nastiuk KL, et al. Infiltrating Myeloid Cells Exert Protumorigenic Actions via Neutrophil Elastase. Mol Cancer Res 2017;15(9):1138–52 doi 10.1158/1541-7786.MCR-17-0003. [PubMed: 28512253]
19. Ho AS, Chen CH, Cheng CC, Wang CC, Lin HC, Luo TY, et al. Neutrophil elastase as a diagnostic marker and therapeutic target in colorectal cancers. Oncotarget 2014;5(2):473–80 doi 10.18632/oncotarget.1631. [PubMed: 24457622]
20. Houghton AM, Rzymkiewicz DM, Ji H, Gregory AD, Egea EE, Metz HE, et al. Neutrophil elastase-mediated degradation of IRS-1 accelerates lung tumor growth. Nat Med 2010;16(2):219–23 doi nm.2084 [pii] 10.1038/nm.2084. [PubMed: 20081861]
21. Wada Y, Yoshida K, Hihara J, Konishi K, Tanabe K, Ukon K, et al. Sivelestat, a specific neutrophil elastase inhibitor, suppresses the growth of gastric carcinoma cells by preventing the release of transforming growth factor-alpha. Cancer Sci 2006;97(10):1037–43 doi 10.1111/j.1349-7006.2006.00278.x. [PubMed: 16918998]
22. Caruso JA, Akli S, Pageon L, Hunt KK, Keyomarsi K. The serine protease inhibitor elafin maintains normal growth control by opposing the mitogenic effects of neutrophil elastase. Oncogene 2015;34(27):3556–67 doi 10.1038/onc.2014.284. [PubMed: 25195861]
23. Vaguliene N, Zemaitis M, Lavinskiene S, Miliauskas S, Sakalauskas R. Local and systemic neutrophilic inflammation in patients with lung cancer and chronic obstructive pulmonary disease. BMC Immunol 2013;14:36 doi 10.1186/1471-2172-14-36. [PubMed: 23919722]
24. Ahn SV, Lee E, Park B, Jung JH, Park JE, Sheen SS, et al. Cancer development in patients with COPD: a retrospective analysis of the National Health Insurance Service-National Sample Cohort in Korea. BMC Pulm Med 2020;20(1):170 doi 10.1186/s12890-020-01194-8. [PubMed: 32539764]
25. Ho CH, Chen YC, Wang JJ, Liao KM. Incidence and relative risk for developing cancer among patients with COPD: a nationwide cohort study in Taiwan. BMJ Open 2017;7(3):e013195 doi 10.1136/bmjopen-2016-013195.
26. Nakayama M, Satoh H, Sekizawa K. Risk of cancers in COPD patients. Chest 2003;123(5):1775–6 doi 10.1378/chest.123.5.1775-a.
27. van Gestel YR, Hoeks SE, Sin DD, Huzeir V, Stam H, Mertens FW, et al. COPD and cancer mortality: the influence of statins. Thorax 2009;64(11):963–7 doi 10.1136/thx.2009.116731. [PubMed: 19720607]
28. Foekens JA, Ries C, Look MP, Gippner-Steppert C, Klijn JG, Jochum M. The prognostic value of polymorphonuclear leukocyte elastase in patients with primary breast cancer. Cancer Res 2003;63(2):337–41. [PubMed: 12543785]
29. Burcham GN, Cresswell GM, Snyder PW, Chen L, Liu X, Crist SA, et al. Impact of prostate inflammation on lesion development in the POET3(+)Pten(+/−) mouse model of prostate carcinogenesis. Am J Pathol 2014;184(12):3176–91 doi 10.1016/j.ajpath.2014.08.021. [PubMed: 25455686]
30. Shang K, Bai YP, Wang C, Wang Z, Gu HY, Du X, et al. Crucial involvement of tumor-associated neutrophils in the regulation of chronic colitis-associated carcinogenesis in mice. PLoS One 2012;7(12):e51848 doi 10.1371/journal.pone.0051848. [PubMed: 23272179]
31. Starcher B, O'Neal P, Granstein RD, Beissert S. Inhibition of neutrophil elastase suppresses the development of skin tumors in hairless mice. J Invest Dermatol 1996;107(2):159–63. [PubMed: 8757756]
32. Albrengues J, Shields MA, Ng D, Park CG, Ambrico A, Poindexter ME, et al. Neutrophil extracellular traps produced during inflammation awaken dormant cancer cells in mice. Science 2018;361(6409) doi 10.1126/science.aao4227.

33. Cools-Lartigue J, Spicer J, McDonald B, Gowing S, Chow S, Giannias B, et al. Neutrophil extracellular traps sequester circulating tumor cells and promote metastasis. J Clin Invest 2013 doi 10.1172/JCI67484.
34. Betts AO. Pathogen-free pigs for industry and research. Proc R Soc Med 1962;55(4):259–62. [PubMed: 13868677]
35. Dobson GP, Letson HL, Biros E, Morris J. Specific pathogen-free (SPF) animal status as a variable in biomedical research: Have we come full circle? EBioMedicine 2019;41:42–3 doi 10.1016/j.ebiom.2019.02.038. [PubMed: 30803932]
36. Belaaouaj A, McCarthy R, Baumann M, Gao Z, Ley TJ, Abraham SN, et al. Mice lacking neutrophil elastase reveal impaired host defense against gram negative bacterial sepsis. Nature medicine 1998;4(5):615–8.
37. Akli S, Van Pelt CS, Bui T, Multani AS, Chang S, Johnson D, et al. Overexpression of the low molecular weight cyclin E in transgenic mice induces metastatic mammary carcinomas through the disruption of the ARF-p53 pathway. Cancer Res 2007;67(15):7212–22 doi 10.1158/0008-5472.CAN-07-0599. [PubMed: 17671189]
38. Chen Y, Kim J, Yang S, Wang H, Wu CJ, Sugimoto H, et al. Type I collagen deletion in alphaSMA(+) myofibroblasts augments immune suppression and accelerates progression of pancreatic cancer. Cancer Cell 2021;39(4):548–65 e6 doi 10.1016/j.ccell.2021.02.007. [PubMed: 33667385]
39. Curtis C, Shah SP, Chin SF, Turashvili G, Rueda OM, Dunning MJ, et al. The genomic and transcriptomic architecture of 2,000 breast tumours reveals novel subgroups. Nature 2012;486(7403):346–52 doi 10.1038/nature10983. [PubMed: 22522925]
40. Pereira B, Chin SF, Rueda OM, Vollan HK, Provenzano E, Bardwell HA, et al. The somatic mutation profiles of 2,433 breast cancers refines their genomic and transcriptomic landscapes. Nat Commun 2016;7:11479 doi 10.1038/ncomms11479. [PubMed: 27161491]
41. Krasnov GS, Kudryavtseva AV, Snezhkina AV, Lakunina VA, Beniaminov AD, Melnikova NV, et al. Pan-Cancer Analysis of TCGA Data Revealed Promising Reference Genes for qPCR Normalization. Front Genet 2019;10:97 doi 10.3389/fgene.2019.00097. [PubMed: 30881377]
42. Cerami E, Gao J, Dogrusoz U, Gross BE, Sumer SO, Aksoy BA, et al. The cBio cancer genomics portal: an open platform for exploring multidimensional cancer genomics data. Cancer Discov 2012;2(5):401–4 doi 10.1158/2159-8290.CD-12-0095. [PubMed: 22588877]
43. Stevens T, Ekholm K, Granse M, Lindahl M, Kozma V, Jungar C, et al. AZD9668: pharmacological characterization of a novel oral inhibitor of neutrophil elastase. The Journal of pharmacology and experimental therapeutics 2011;339(1):313–20 doi 10.1124/jpet.111.182139. [PubMed: 21791628]
44. Alcaraz M-L, Briggner L-E, Klingstedt P, Tomas, Loenn H, Roland, Nicklasson H, Nixon R, Anthony, et al.; World Intellectual Property Organization, assignee. Preparation of pyrazole derivatives for treatment of COPD. US patent WO2010/094964 A1. 2010–08-26.
45. Fouret P, du Bois RM, Bernaudin JF, Takahashi H, Ferrans VJ, Crystal RG. Expression of the neutrophil elastase gene during human bone marrow cell differentiation. J Exp Med 1989;169(3):833–45. [PubMed: 2538548]
46. Makaryan V, Zeidler C, Bolyard AA, Skokowa J, Rodger E, Kelley ML, et al. The diversity of mutations and clinical outcomes for ELANE-associated neutropenia. Curr Opin Hematol 2015;22(1):3–11 doi 10.1097/MOH.0000000000000105. [PubMed: 25427142]
47. Lerman I, Hammes SR. Neutrophil elastase in the tumor microenvironment. Steroids 2018;133:96–101 doi 10.1016/j.steroids.2017.11.006. [PubMed: 29155217]
48. Lin EY, Jones JG, Li P, Zhu L, Whitney KD, Muller WJ, et al. Progression to malignancy in the polyoma middle T oncoprotein mouse breast cancer model provides a reliable model for human diseases. Am J Pathol 2003;163(5):2113–26 doi 10.1016/S0002-9440(10)63568-7. [PubMed: 14578209]
49. Guy CT, Cardiff RD, Muller WJ. Induction of mammary tumors by expression of polyomavirus middle T oncogene: a transgenic mouse model for metastatic disease. Mol Cell Biol 1992;12(3):954–61. [PubMed: 1312220]

50. Goldstein RH, Weinberg RA, Rosenblatt M. Of mice and (wo)men: mouse models of breast cancer metastasis to bone. J Bone Miner Res 2010;25(3):431–6 doi 10.1002/jbmr.68. [PubMed: 20200984]
51. Fantozzi A, Christofori G. Mouse models of breast cancer metastasis. Breast Cancer Res 2006;8(4):212 doi 10.1186/bcr1530. [PubMed: 16887003]
52. Heinz A. Elastases and elastokines: elastin degradation and its significance in health and disease. Crit Rev Biochem Mol Biol 2020;55(3):252–73 doi 10.1080/10409238.2020.1768208. [PubMed: 32530323]
53. Stone PJ, Gottlieb DJ, O'Connor GT, Ciccolella DE, Breuer R, Bryan-Rhadfi J, et al. Elastin and collagen degradation products in urine of smokers with and without chronic obstructive pulmonary disease. Am J Respir Crit Care Med 1995;151(4):952–9 doi 10.1164/ajrccm.151.4.7697272. [PubMed: 7697272]
54. Hollern DP, Swiatnicki MR, Andrechek ER. Histological subtypes of mouse mammary tumors reveal conserved relationships to human cancers. PLoS Genet 2018;14(1):e1007135 doi 10.1371/journal.pgen.1007135.
55. Rekad Z, Izzi V, Lamba R, Ciais D, Van Obberghen-Schilling E. The alternative matrisome: Alternative splicing of ECM proteins in development, homeostasis and tumor progression. Matrix Biol 2022;111:26–52 doi 10.1016/j.matbio.2022.05.003. [PubMed: 35537652]
56. Mi H, Muruganujan A, Thomas PD. PANTHER in 2013: modeling the evolution of gene function, and other gene attributes, in the context of phylogenetic trees. Nucleic Acids Res 2013;41(Database issue):D377–86 doi 10.1093/nar/gks1118. [PubMed: 23193289]
57. Shao X, Taha IN, Clauser KR, Gao YT, Naba A. MatrisomeDB: the ECM-protein knowledge database. Nucleic Acids Res 2020;48(D1):D1136–D44 doi 10.1093/nar/gkz849. [PubMed: 31586405]
58. Erdogan B, Ao M, White LM, Means AL, Brewer BM, Yang L, et al. Cancer-associated fibroblasts promote directional cancer cell migration by aligning fibronectin. J Cell Biol 2017;216(11):3799–816 doi 10.1083/jcb.201704053. [PubMed: 29021221]
59. Clancy DM, Sullivan GP, Moran HBT, Henry CM, Reeves EP, McElvaney NG, et al. Extracellular Neutrophil Proteases Are Efficient Regulators of IL-1, IL-33, and IL-36 Cytokine Activity but Poor Effectors of Microbial Killing. Cell Rep 2018;22(11):2937–50 doi 10.1016/j.celrep.2018.02.062. [PubMed: 29539422]
60. Liu J, Lichtenberg T, Hoadley KA, Poisson LM, Lazar AJ, Cherniack AD, et al. An Integrated TCGA Pan-Cancer Clinical Data Resource to Drive High-Quality Survival Outcome Analytics. Cell 2018;173(2):400–16 e11 doi 10.1016/j.cell.2018.02.052. [PubMed: 29625055]
61. Polverino E, Rosales-Mayor E, Dale GE, Dembowsky K, Torres A. The role of neutrophil elastase inhibitors in lung diseases. Chest 2017;152(2):249–62. [PubMed: 28442313]
62. Gunawardena KA, Gullstrand H, Perrett J. Pharmacokinetics and safety of AZD9668, an oral neutrophil elastase inhibitor, in healthy volunteers and patients with COPD. Int J Clin Pharmacol Ther 2013;51(4):288–304 doi 10.5414/CP201674. [PubMed: 23391369]
63. Kuna P, Jenkins M, O'Brien CD, Fahy WA. AZD9668, a neutrophil elastase inhibitor, plus ongoing budesonide/formoterol in patients with COPD. Respir Med 2012;106(4):531–9 doi 10.1016/j.rmed.2011.10.020. [PubMed: 22197578]
64. Vogelmeier C, Aquino TO, O'Brien CD, Perrett J, Gunawardena KA. A randomised, placebo-controlled, dose-finding study of AZD9668, an oral inhibitor of neutrophil elastase, in patients with chronic obstructive pulmonary disease treated with tiotropium. COPD 2012;9(2):111–20 doi 10.3109/15412555.2011.641803. [PubMed: 22458939]
65. Kirsten AM, Forster K, Radeczky E, Linnhoff A, Balint B, Watz H, et al. The safety and tolerability of oral AZD5069, a selective CXCR2 antagonist, in patients with moderate-to-severe COPD. Pulm Pharmacol Ther 2015;31:36–41 doi 10.1016/j.pupt.2015.02.001. [PubMed: 25681277]
66. Cui C, Chakraborty K, Tang XA, Zhou G, Schoenfelt KQ, Becker KM, et al. Neutrophil elastase selectively kills cancer cells and attenuates tumorigenesis. Cell 2021;184(12):3163–77 e21 doi 10.1016/j.cell.2021.04.016. [PubMed: 33964209]

67. Burn GL, Foti A, Marsman G, Patel DF, Zychlinsky A. The Neutrophil. Immunity 2021;54(7):1377–91 doi 10.1016/j.immuni.2021.06.006. [PubMed: 34260886]

68. Carnevale S, Ghasemi S, Rigatelli A, Jaillon S. The complexity of neutrophils in health and disease: Focus on cancer. Semin Immunol 2020;48:101409 doi 10.1016/j.smim.2020.101409.

69. Hartman MA, Spudich JA. The myosin superfamily at a glance. J Cell Sci 2012;125(Pt 7):1627–32 doi 10.1242/jcs.094300. [PubMed: 22566666]

70. Woolner S, Bement WM. Unconventional myosins acting unconventionally. Trends Cell Biol 2009;19(6):245–52 doi 10.1016/j.tcb.2009.03.003. [PubMed: 19406643]

71. Deryugina E, Carre A, Ardi V, Muramatsu T, Schmidt J, Pham C, et al. Neutrophil Elastase Facilitates Tumor Cell Intravasation and Early Metastatic Events. iScience 2020;23(12):101799 doi 10.1016/j.isci.2020.101799.

72. Wada Y, Yoshida K, Tsutani Y, Shigematsu H, Oeda M, Sanada Y, et al. Neutrophil elastase induces cell proliferation and migration by the release of TGF-alpha, PDGF and VEGF in esophageal cell lines. Oncol Rep 2007;17(1):161–7. [PubMed: 17143494]

73. Kuravi SJ, Bevins A, Satchell SC, Harper L, Williams JM, Rainger GE, et al. Neutrophil serine proteases mediate inflammatory cell recruitment by glomerular endothelium and progression towards dysfunction. Nephrol Dial Transplant 2012;27(12):4331–8 doi 10.1093/ndt/gfs180. [PubMed: 22785107]

74. Li Z, Wang C, Jiao X, Lu Y, Fu M, Quong AA, et al. Cyclin D1 regulates cellular migration through the inhibition of thrombospondin 1 and ROCK signaling. Mol Cell Biol 2006;26(11):4240–56 doi 10.1128/MCB.02124-05. [PubMed: 16705174]

75. Stockley R, De Soyza A, Gunawardena K, Perrett J, Forsman-Semb K, Entwistle N, et al. Phase II study of a neutrophil elastase inhibitor (AZD9668) in patients with bronchiectasis. Respir Med 2013;107(4):524–33 doi 10.1016/j.rmed.2012.12.009. [PubMed: 23433769]

76. Stevens T, Ekholm K, Granse M, Lindahl M, Kozma V, Jungar C, et al. AZD9668: pharmacological characterization of a novel oral inhibitor of neutrophil elastase. The Journal of pharmacology and experimental therapeutics 2011;339(1):313–20 doi 10.1124/jpet.111.182139. [PubMed: 21791628]

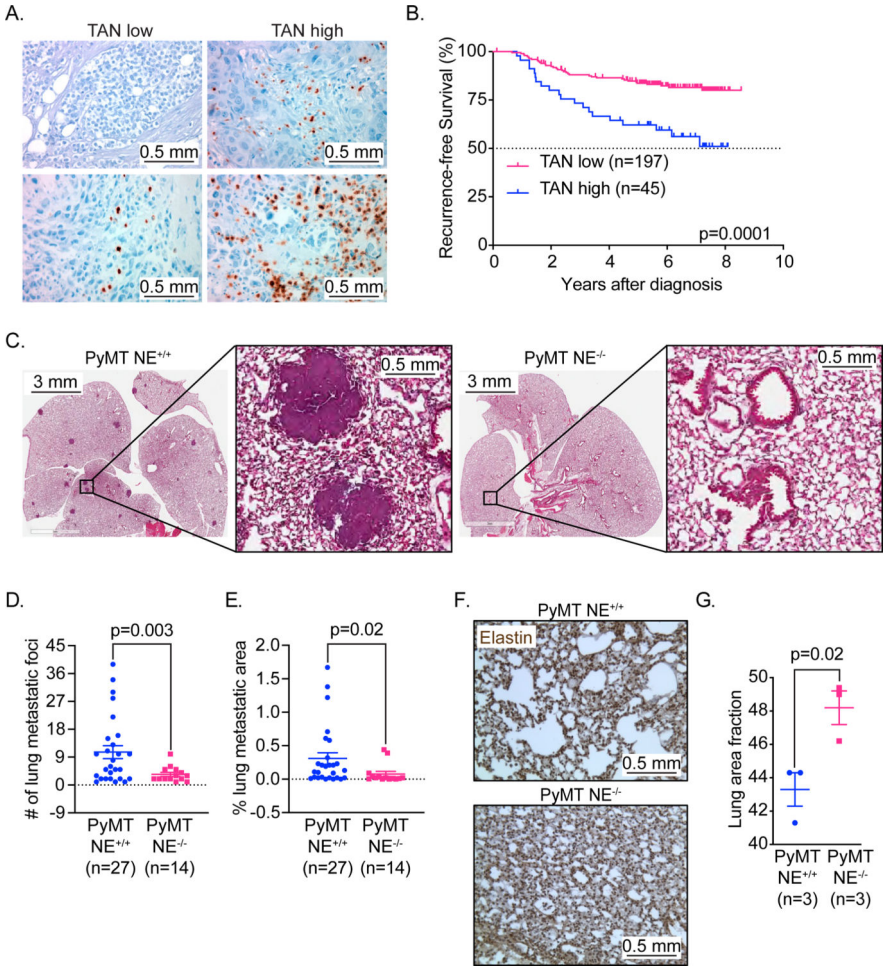

Figure 1: Lack of neutrophil elastase (NE) predicts longer recurrence-free survival in breast cancer patients and inhibits breast cancer metastasis in the PyMT model of breast cancer.

(A) Representative 20X photomicrographs of NE IHC staining of invasive breast carcinoma (human) with negative (top, left), low (bottom, left) and high (top and bottom, right depicting lower and upper limits of high) amounts of tumor associated neutrophils (TANs). Scale bar 0.5 mm. (B) Kaplan-Meier plots for Recurrence Free Survival (RFS) in breast cancer patients from MDACC (n=242) segregated by expression of NE. (C) Representative images in low (1X, left panels) and high (6X, right panels) magnification of H&E-stained lung tissue of endpoint (12–14 weeks age) PyMT NE+/+ & PyMT NE−/− mice. Scale bar 3mm and 0.5 mm. (D) Total number of metastatic foci in PyMT NE+/+ (N=27) & PyMT NE−/− (N=14) mice, at endpoint (12–14 weeks age). (E) Lung metastatic index in PyMT NE+/+ (N=27) & PyMT NE−/− (N=14) mice, at endpoint (12–14 weeks age). (F) Representative images of elastin-stained lungs in PyMT NE+/+ and PyMT NE−/− mice at 12 weeks of age. NE mediated cleavage of elastin is quantified for each set of genotypes in (G). Scale bar 0.5 mm.

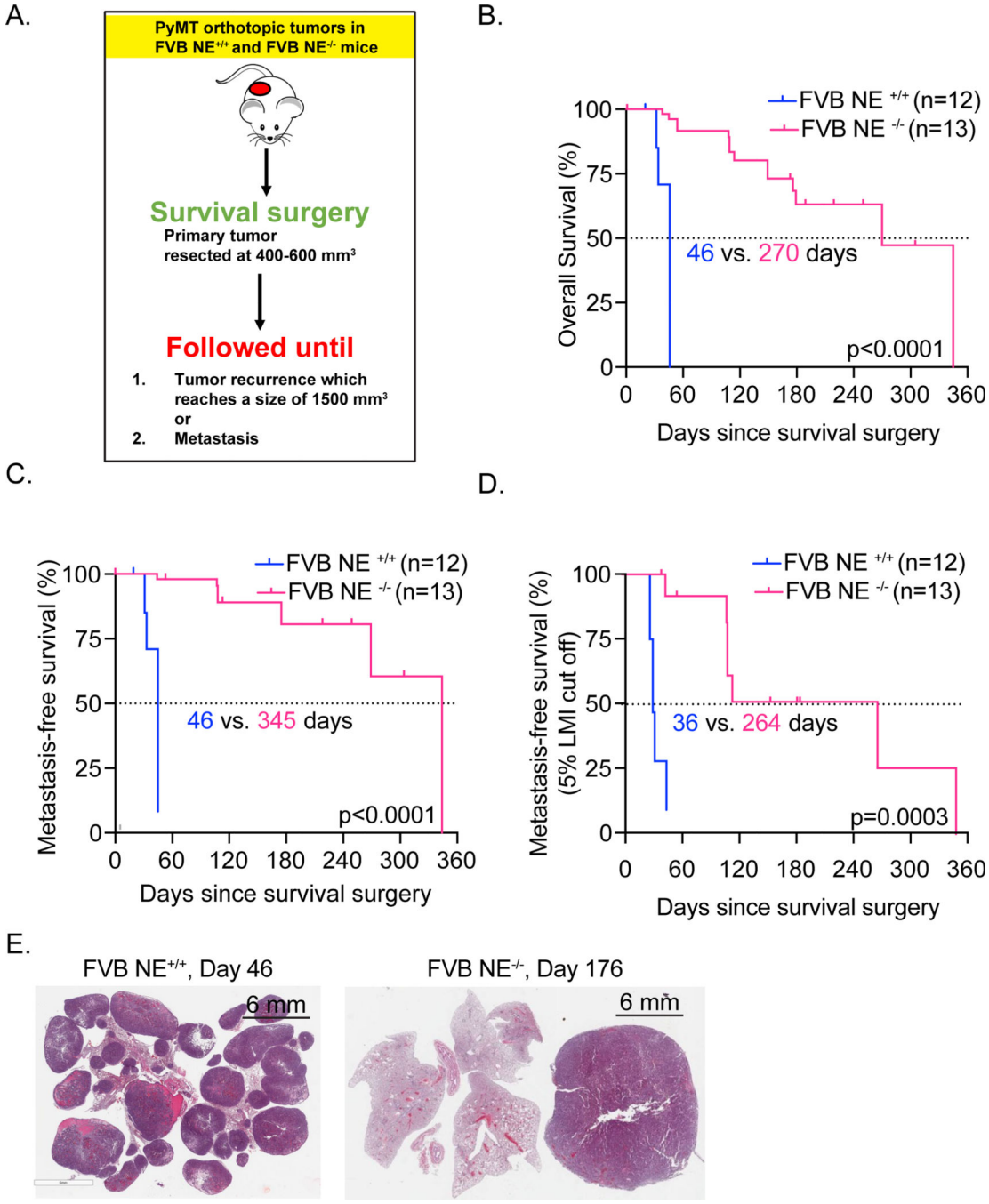

Figure 2: Knockout of NE extends metastasis-free survival in the PyMT model of breast cancer.

(A) Experimental design for assessing survival in FVB NE+/+ and FVB NE−/− mice, bearing orthotopic PyMT tumors. (B) Overall survival and (C) Metastasis-free survival in N=12 FVB NE+/+ mice and N=13 FVB NE−/− mice. (D) Lung metastatic index (LMI) plotted as a function of time in N=12 FVB NE+/+ mice and N=13 FVB NE−/− mice. Events were called using 5% lung metastatic index (LMI) as the cut-off. (E) Representative H&E stained lung sections resected from an FVB NE+/+ mouse on day 46 and FVB NE−/− mouse on day 176, at endpoint. Scale bar 6mm.

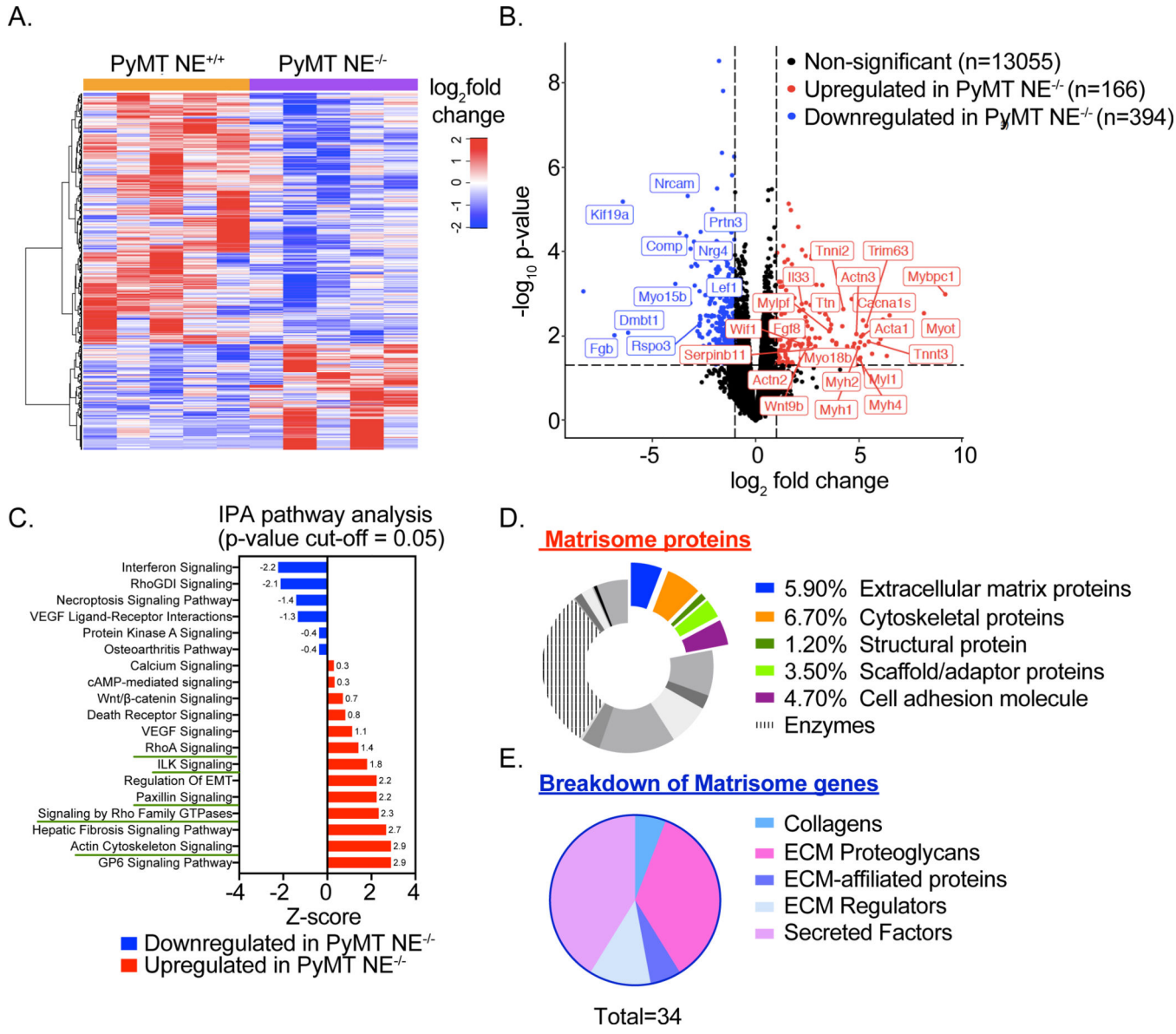

Figure 3: Differential cytoskeleton signaling can distinguish PyMT NE+/+ and PyMT NE−/− tumors.

RNA-seq was performed in endpoint (12–14 weeks) tumors obtained from PyMT NE+/+ (N=5) and PyMT NE−/− (N=5) mice. (A) Heat map and (B) Volcano plot shows that 560 genes (cut-off = p<0.05 and 2-fold change in expression) were differentially expressed genes (DEGs) between the two cohorts. The top 32 genes are highlighted in the volcano plot. (C) Ingenuity Pathway Analysis (IPA) was performed using the 560 DEGs and pathways that were significantly up- or down-regulated are plotted as a function of their Z-score. (D) The 560 DEGs were subject to Gene Ontology (GO) analysis and matrisome proteins were identified as the most enriched class of proteins in the PyMT NE−/− tumors. The pie-chart shows the breakdown of sub-categories of the matrisome proteins identified. (E) Classifying the matrisome proteins at the transcriptomic level revealed that the majority of the DEGs identified were secreted factors and ECM proteoglycans.

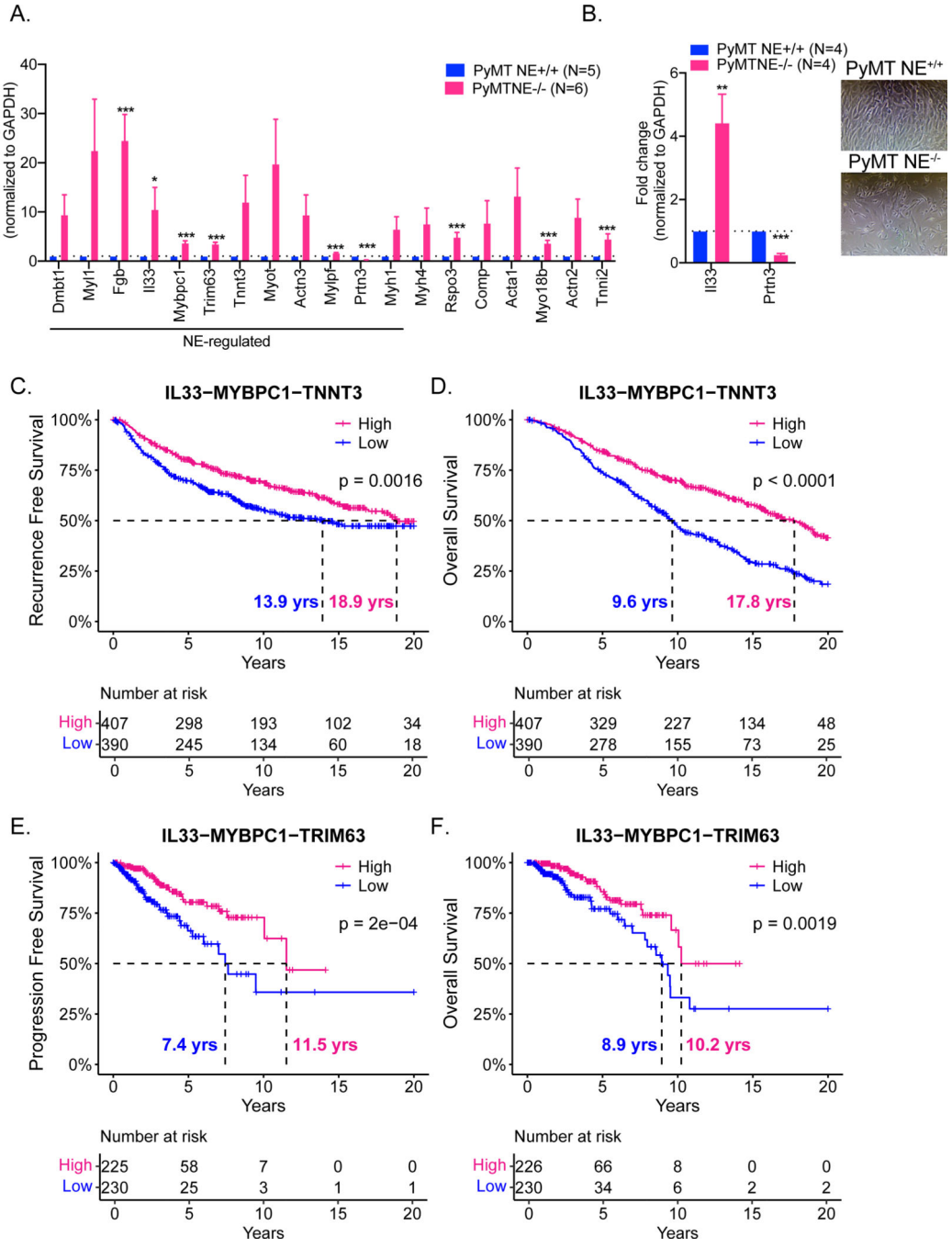

Figure 4: NE-mediated transcriptomic changes prime cancer cells to metastasize in PyMT NE+/+ tumors.

(A) qRT-PCR analysis was performed in a validation set of N=5 PyMT NE+/+ and N=6 PyMT NE−/− tumors. Of the top 32 genes, a 19-gene signature was identified, confirming the RNA-seq data. Significantly altered genes were identified by Student's t-test for pairwise comparisons (* p<0.05, ** p<0.01, ***p<0.001) (B) Tumor associated fibroblasts (CD140+ve) were sorted from live PyMT NE+/+ (n=4) and PyMT NE−/− (n=4) tumors. CD140+ve fibroblasts were then subject to RNA isolation and qRT-PCR analysis for all 19 genes. Using the 12 NE regulated genes, (C, D) METABRIC (39,40), and (E, F) TCGA (60)

databases were interrogated for recurrence-free survival (RFS) and overall survival (OS) (METABRIC) and for progression-free survival (PFS) and OS (TCGA) in breast cancer patients. For each gene, the median expression was used as a cutoff to define high and low groups. A NE−/− specific gene signature was then generated using the genes that showed significant differences in OS and RFS/PFS for individual genes, in each database (Supplementary Figure S7). Only those patients with either all high or all low expression for each 3-gene signature were evaluated for RFS or PFS and OS. Improved outcome correlated with high expression of all genes and was presented as a combined signature for each database.

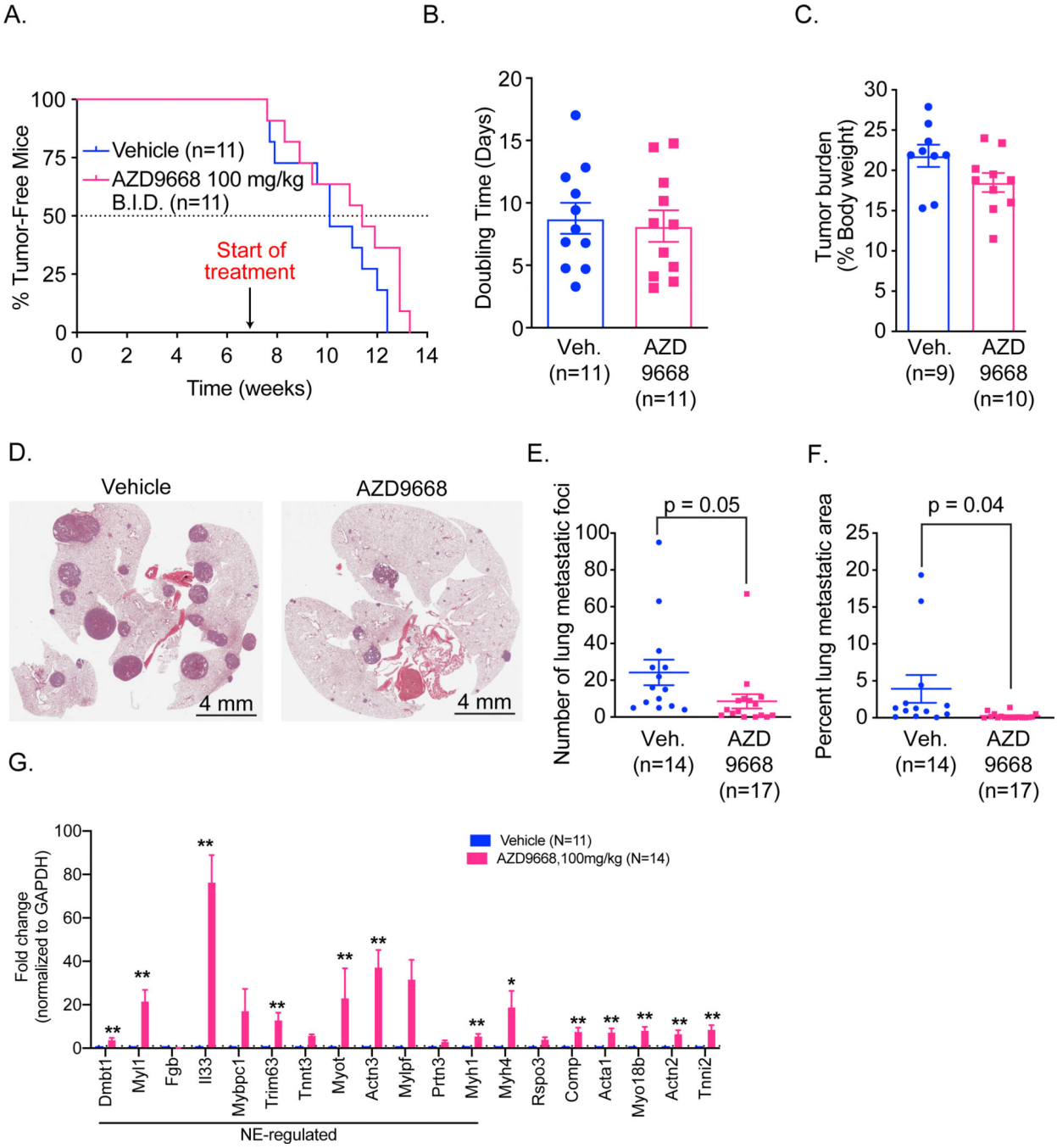

Figure 5: NE-specific inhibitor AZD9668 can phenocopy NE knockout in the PyMT breast cancer model.

7-week old PyMT NE+/+ mice were treated with either vehicle (N=11) or 100mg/kg AZD9668 (N=11), by intraperitoneal (IP) injection, B.I.D. (*bis in die*, twice a day), daily for 6–7 weeks, starting at week 7. (A) Percent of tumor-free mice, up to the endpoint of 12–14 weeks is shown. (B) Doubling time and (C) Total tumor mass for each mouse treated in (A) is shown. (D) Representative images of H&E-stained lung tissue of mice treated either with vehicle or 100mg/kg AZD9668 is shown. Lungs were collected at endpoint (12–14 weeks age) and analyzed for metastasis. Scale bar 4mm. (E) Total number of lung

metastatic foci and D) lung metastatic index in PyMT NE+/+ treated with vehicle (N=14) & AZD9668 (N=17) treated mice, at the endpoint (12–14 weeks old). (G) qRT-PCR analysis for the 19-gene signature identified in Figure 4A was interrogated in tumors from A) Genes significantly altered as a result of AZD9668 treatments were by identified Student's t-test for pairwise comparisons (* $p<0.05$, ** $p<0.01$).

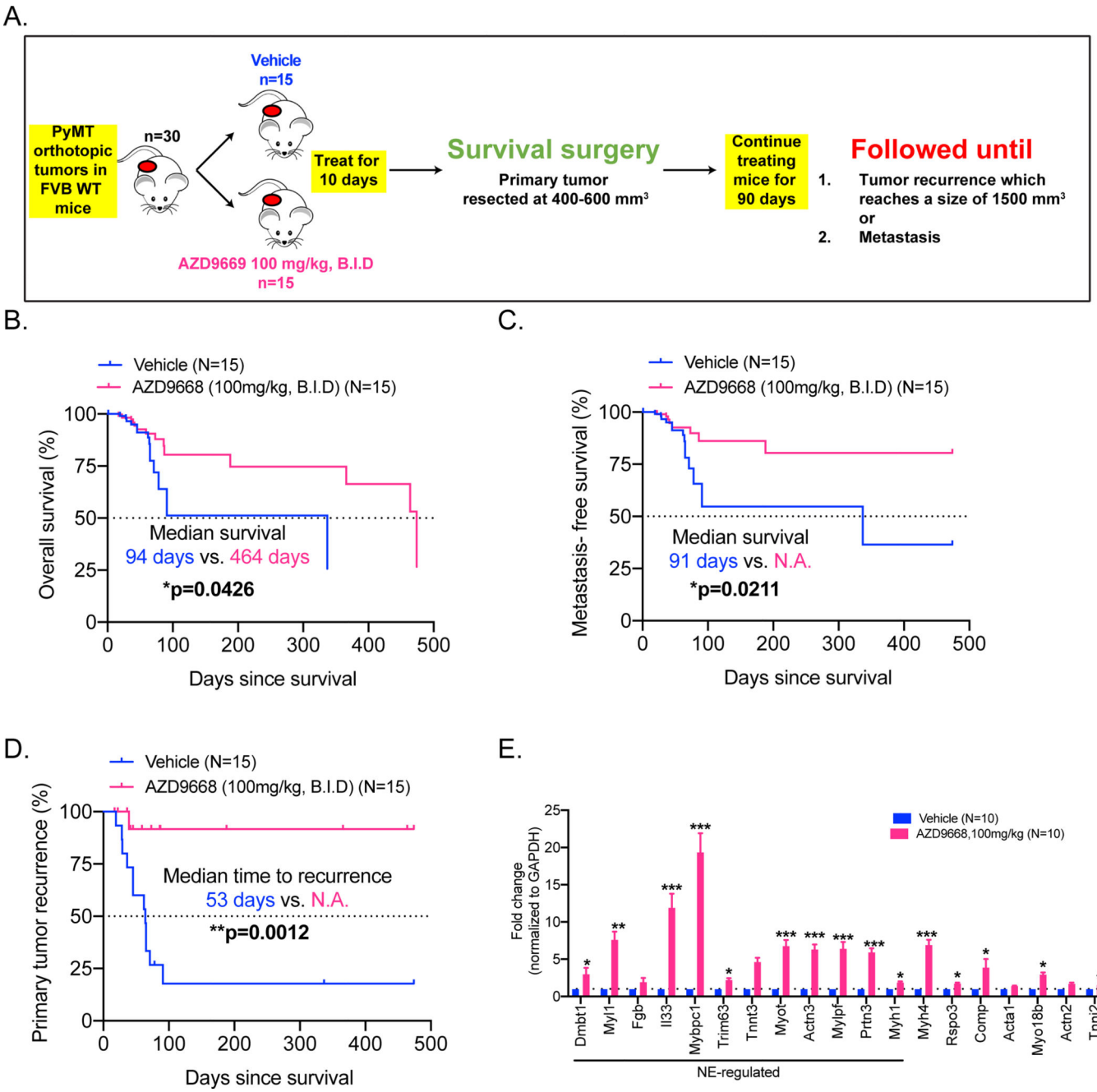

Figure 6: AZD9668 extends RFS in FVB NE+/+ mice bearing PyMT tumors.

A) Experimental design for assessing survival in FVB WT bearing orthotopic PyMT tumors, treated with either vehicle (N=15) or AZD9668, 100mg/kg B.I.D (N=15) (B) Overall survival and (C) Metastasis-free survival (MFS) in mice, at endpoint (N.A.=Not achieved). Endpoint was defined as death due to distant metastasis. (D) Primary tumor-recurrence incidence (%) was evaluated in the mice described in A). (E) qRT-PCR analysis for the 19-gene signature identified in Figure 4A was interrogated in tumors from A). Genes

significantly altered as a result of AZD9668 treatments were by identified Student's t-test for pairwise comparisons (* $p<0.05$, ** $p<0.01$, *** $p<0.001$).